Astronomy & Astrophysics manuscript no. final˙radiozcosmos
November 3, 2009
© ESO 2009

arXiv:0911.0523v1 [astro-ph.CO] 3 Nov 2009

Properties and environment of Radio Emitting Galaxies in the VLA-zCOSMOS survey *

S. Bardelli[1], E. Schinnerer[2], V. Smolčic[3], G. Zamorani[1], E. Zucca[1], M.Mignoli[1], C.Halliday[4], K.Kovač[5], P.Ciliegi[1], K.Caputi[5], A.M. Koekemoer[6], A.Bongiorno[7], M.Bondi[8], M.Bolzonella[1], D.Vergani[1], L.Pozzetti[1], C.M.Carollo[5], T.Contini[9], J.-P.Kneib[10], O.Le Fèvre[10], S.Lilly[5], V.Mainieri[11], A.Renzini[12], M.Scodeggio[13], G.Coppa[1], O.Cucciati[10], S.de la Torre[14], L.de Ravel[10], P.Franzetti[13], B.Garilli[13], A.Iovino[14], P.Kampczyk[5], C.Knobel[5], F.Lamareille[9], J.-F.Le Borgne[9], V.Le Brun[10], C.Maier[5], R.Pellò[9], Y.Peng[5], E.Perez-Montero[9,27], E.Ricciardelli[12], J.D.Silverman[5], M.Tanaka[11], L.Tasca[13], L.Tresse[10], U.Abbas[15], D.Bottini[13], A.Cappi[1], P.Cassata[16], A.Cimatti[17], L.Guzzo[14], A.Leauthaud[18], D.Maccagni[13], C.Marinoni[19], H.J.McCracken[20], P.Memeo[13], B.Meneux[7,28], P.Oesch[5], C.Porciani[21], R.Scaramella[22], P.Capak[23], D.Sanders[24], N.Scoville[3], Y.Taniguchi[25], and K.Jahnke[26]

(Affiliations can be found after the references)

Received – –; accepted – –

ABSTRACT

Aims. We investigate the properties and the environment of radio sources with optical counterpart from the combined VLA-COSMOS and zCOSMOS samples. The advantage of this sample is the availability of optical spectroscopic information, high quality redshifts, and accurate density determination.

Methods. By comparing the star formation rates estimated from the optical spectral energy distribution with those based on the radio luminosity, we divide the radio sources in three families, passive AGN, non-passive AGN and star forming galaxies. These families occupy specific regions of the 8.0-4.5 μm infrared color- specific star formation plane, from which we extract the corresponding control samples.

Results. Only the passive AGN have a significantly different environment distribution from their control sample. The fraction of radio-loud passive AGN increases from $\sim 2\%$ in underdense regions to $\sim 15\%$ for overdensities $(1+\delta)$ greater than 10. This trend is also present as a function of richness of the groups hosting the radio sources. Passive AGN in overdensities tend to have higher radio luminosities than those in lower density environments. Since the black hole mass distribution is similar in both environments, we speculate that, for low radio luminosities, the radio emission is controlled (through fuel disponibility or confinement of radio jet by local gas pressure) by the interstellar medium of the host galaxy, while in other cases it is determined by the structure (group or cluster) in which the galaxy resides.

Key words. Galaxies:fundamental parameters - Galaxies:general - Galaxies:luminosity function, mass function - Radio continuum:galaxies

1. Introduction

Radio sources have been traditionally classified into two broad classes depending upon their emission mechanism: AGN-driven emission has been supposed for early type galaxies, while a star forming origin of the radio power has been invoked for late type galaxies (Condon, 1992). However, not all optical galaxies exhibit radio emission (at least at the depth of current surveys) and it is important to investigate the physical mechanism which triggers this emission. For AGN-induced activity, the difference between radio quiet and radio loud galaxies is naturally connected with the availability of fuel for the central engine, the black hole mass, and its emission efficiency (see e.g. Shabala et al., 2008, and references therein), while for star forming objects it is closely related to the strength of the star formation episode.

Heating by a central AGN is also thought to be important for the host galaxy evolution, providing the energy to stop the central cooling that drives gas to the central black hole in an intermittent feedback mechanism dubbed ”radio mode” (see Croton et al., 2006; Ciotti Ostriker & Proga, 2009). The same intermittent mechanism is indirectly observed as bubbles in the intra-cluster medium (Birzan et al., 2004) or in the restarted activity of radio sources (Venturi Dallacasa & Stefanachi, 2004; Bardelli et al., 2002). This heating emission is thought also to be able to suppress the star formation and to be an important mechanism for creating the galaxy color bimodality (Croton et al., 2006). Moreover, it is a fact that many radio AGN reside in early type galaxies (Ledlow & Owen, 1996), a class of objects which are preferentially found in high density environments.

It has been proposed that cluster/group mergers, galaxy-galaxy mergings or at least tidal disturbance caused by close encounters between galaxies would increase radio activity. For early type galaxies, these phenomena could drive gas more efficently toward the center, while for late type galaxies, these encounters would trigger and/or enhance star formation (see e.g. Bekki, 1999; Vollmer et al., 2001). The radio luminosity of the AGN also depends on the interaction of the jet coming from the black hole with the surrounding gas of the host galaxy and/or of the hosting cluster (see e.g. Shabala et al., 2008, and references therein). For these reasons, some degree of dependence of radio activity on the environment is expected. Although the problem is clear from the qualitative description, controversial results are present in the literature and for mainly two reasons.

Send offprint requests to: S.Bardelli sandro.bardelli@oabo.inaf.it

* based on data obtained with the European Southern Observatory Very Large Telescope, Paranal, Chile, program 175.A-0839 and VLA-Large Program VLA-AS0801

First of all, very few papers are primarily based on radio data. Usually, papers in the literature consider AGN selected on the basis of their optical (mostly estimated from line diagnostics) or X-ray activity (see Kauffmann et al., 2004, and references therein). It seems that the family of optical/X-ray AGN inhabits similar environments to non-active galaxies, with a preference for lower densities at higher stellar masses (Kauffmann et al., 2004; Silverman et al., 2009b). However, Best et al. (2005) claim that the phenomena generating the emission lines and the radio emission are statistically independent, even if recent results indicate that radio loud emission line AGN favour higher densities than radio quiet ones (Kauffmann Heckman & Best, 2008) (see also Caputi et al., 2009, for a study in the IR). Secondly, only specific environments have been considered, mainly clusters or groups (Miller et al., 2002; Hill & Lilly, 1991; Giacintucci et al., 2004), lacking therefore the coverage of a large dynamical range in densities.

The first paper that studied in a complete statistical way, both from the radio and optical side, the environment of radio galaxies was that of Best (2004) . This paper uses data from 2dF Galaxy Redshift Survey (Colless et al., 2001) and the NRAO VLA Sky Survey (Condon et al., 1998) with a well defined estimator of density, i.e. the projected density of the 10^{th} nearest neighbor. Moreover, groups (and clusters) are found with the standard friend-of-friends detection method. The redshift range is $0.02 < z < 0.1$. The general result is that radio-selected star forming galaxies decrease in number with increasing overdensity, while objects with AGN activity exhibit little dependence upon the local density, except at the very low densities, where the probability to find these objects decreases significantly. Best (2004) claims also that the larger scale (i.e. on the scales typical of groups and clusters) is more important than the smaller scale (typical of galaxy pairs or companions) to determine the AGN radio emission. Star forming galaxies do not exhibit dependence on environment at scales larger than one Mpc (Kauffmann et al., 2004).

In this paper we investigate the environment properties of the radio sources present in the zCOSMOS survey using a set of well defined density estimators in the redshift range [0.1-0.9]. In Section 2 we present the used data and the estimators for various environments; in Section 3 we describe the method adopted to separate galaxies with radio emission induced by AGN from that induced by star formation and the definition of the control samples. In Section 4 we discuss the differences between the various samples, while in Section 5 we present the dependences on environment. In Section 6 the luminosity distributions and radio-optical ratio for a specific class of radio AGN are shown and in Section 7 we discuss the results. The adopted cosmology has $\Omega_m = 0.25, \Omega_\Lambda = 0.75$ and $H_0 = 70$ km s^{-1} Mpc^{-1}.

Throughout the paper we adopted the term ”radio galaxy” for galaxies hosting a radio source, independently of the physical nature of the emission.

2. Data and density estimators

To select the optical sample, we used the zCOSMOS Bright survey, a redshift survey with a magnitude selection of $I_{AB} < 22.5$ (Lilly et al., 2007, 2009) that has been undertaken in the 1.7 deg^2 of the COSMOS field (Scoville et al., 2007), imaged by the Hubble Space Telescope / Advanced Camera for Surveys F814W I-band (Koekemoer et al., 2007).

The observations are being carried out with the 8-meter ESO Very Large Telescope using VIMOS, a multi-slit spectrograph with a resolution of $R \sim 600$, resulting in an r.m.s. accuracy on the velocity determinations of $\sim$ 110 km s^{-1} (Lilly et al., 2007, 2009)

This paper is based on the first $\sim 10,000$ spectra, which have a rather non-uniform sampling pattern (see Figure 5 in Lilly et al., 2009) over an area of 1.40 deg^2 and an average sampling rate of $\sim$ 33%. From this sample, we extracted a ”statistical sample” of 8481 galaxies with high quality redshift determination ($flag > 1.5$) and excluding broad line AGN. Note that within our redshift limit of 0.9 adopted in the following analysis, the number of broad line AGN is 17, of which 3 are radio loud.

Absolute magnitudes were computed following the method of Ilbert et al. (2005) from the COSMOS photometry (see Zucca et al., 2009), which covers a wide range of wavelength from the UV to the NIR. This method computes the rest-frame absolute magnitudes using the nearest observed band (at the redshift of the galaxy) plus a correction derived from a template fit and is the least template dependent possible.

We used stellar masses (M_{star})and star formation rates (SFRs) computed by Bolzonella et al. (2009) using *Hyperzmass* (see details in Bolzonella et al., 2009; Pozzetti et al., 2007) by means of a spectral energy distribution fit to the photometric data. The method uses the Bruzual & Charlot (2003) library and the Chabrier (2003) Initial Mass Function. The library provides a model for a simple stellar population and its evolution in 220 age steps. From this database *Hyperzmass* imposes a set of 10 exponentially decreasing star formation histories (with e-folding times ranging from 0.1 to 30 Gyrs plus a model of continuous star formation) in order to fit the photometric data. We asssume the values of stellar mass and star formation rate of the best fit template. The typical statistical error on the stellar masses is estimated to be $\sim$ 0.20 dex.

The usually adopted conversions between radio luminosity and star formation rate are based on the Salpeter (1955) initial mass function and for this reason we corrected our $logM_{star}$ and $log(SFR)$ by adding 0.23 and 0.19, respectively, which are the median differences of the two quantities computed with the two initial mass functions.

For the radio band we used the VLA-COSMOS survey, a large project consisting of 23 pointings in an area of 1.4 x 1.4 square degrees (Schinnerer et al., 2007; Bondi et al., 2008). The resolution is 1.5 x 1.4 arcsec^2 and the survey, which has a mean r.m.s. of $\sim 10.5\,\mu$Jy, detected 2501 sources at more than 5σ.

Ciliegi et al. (2009) correlated this sample with the COSMOS optical samples (Capak et al., 2007), finding 2060 radio sources with optical counterparts. We correlate the zCOSMOS ”statistical sample” with the VLA-COSMOS sample obtaining a final radio sample of 315 radio galaxies observed spectroscopically out of the 1231 radio sources with $I_{AB} < 22.5$. Note that our radio data ampling rate is slightly smaller than the average zCOSMOS sampling rate because the zCOSMOS survey does not cover the entire VLA-COSMOS area.

Radio luminosities have been computed assuming that the radio spectrum is a power law function (defined by $S \propto \nu^{\alpha}$) with a slope $\alpha = -0.7$.

We used the density estimtes computed by Kovač et al. (2009) using the ZADE algorithm, which maximizes the statistical robustness of the estimators using both the spectroscopic and the photometric redshift samples. The algorithm offers the densities computed for each galaxy both as a function of the distance of the nth - nearest neighbour and in spheres of fixed comoving radius. These densities are also computed by weighting the galaxies by either their B band luminosities or stellar masses. As tracers of the density field, both galaxies of a flux limited and volume limited sample have been used.

The method has been tested on mock cosmological simulations, by extracting samples with the same observational limits as zCOSMOS. The overdensities were found to be correctly estimated at all redshifts with a slight ($\sim$ 20%) underestimate of the real value at low densities, corresponding to $(1 + \delta) < 0.1$ (where $\delta = \rho - <\rho> / <\rho>$). In the following, we will use the densities derived with the nearest neighbor approach.

In addition, the zCOSMOS optically-selected group catalog (Knobel et al., 2009) offers a complementary perspective on the role of environment (Iovino et al., 2009). These groups have been extracted using a combination of the friends-of-friends method with a Voronoi tesselation density estimator on the zCOSMOS spectroscopic catalogue. The method, applied to the statistical sample, detected $\sim$ 800 groups, 103 of which have more than 5 members. The fraction of galaxies in group is $\sim$ 20% with some dependence on redshift. Estimates of the group richness have been calculated using the number of galaxies of the volume limited sample, considered as proxies for the total richness of groups.

3. AGN versus Star Forming galaxies in environmental studies.

There are essentially two steps in studying environmental effects for radio sources: the division of radio sources according to AGN and star forming induced radio emission and the definition of coherent control samples. In fact, it is already known that radio AGN reside mostly in early type galaxies and therefore their overdensity distribution has to be compared only with that of radio quiet early type galaxies, otherwise any possible difference observed in environment could just be due to the optical morphology-density relation (Dressler, 1980).

However, a sharp division between AGN and SF galaxies in some cases has little physical meaning, because we know that both phenomena are commonplace in a number of galaxies (see e.g. Silverman et al., 2009a) and it is therefore difficult to determine the fraction of the radio flux that originates from AGN and/or from the star formation activity.

For AGN/SF galaxy luminosity function studies (e.g. Bardelli et al., 2009; Smolčic et al., 2009a,b), the aim is to count the total number of AGN (or star forming galaxies) and for these studies it is correct to consider all objects exhibiting AGN (SF) activity, regardless of its relative contribution to the radio flux. For density studies the situation is slightly different. In this case, we ask whether the environment has (or not) any effect in triggering radio emission from AGN or star formation and it is not easy to reach a conclusion in those composite objects, considering that the trigger mechanisms are likely very different.

In other words, if a class of radio sources exhibits an environmental dependence, is this related to its star forming or AGN part of the flux?

In the following, we present a method for selecting subsamples in such a way that the ”radio AGN sample” contains radio sources for which the AGN emission is at least about one order of magnitude higher than that expected from the star formation. Therefore, our definition of radio AGN is ”an object for which the radio emission is largely dominated by the emission of the central engine”.

With this definition, the optical AGN as defined on the basis of emission line ratios, will be included in the star forming galaxies sample if they have a low ratio of AGN/SF radio flux. This inclusion is supported by a) the independence of emission line and radio emission (Best et al., 2005), at least for low luminosity AGN as ours, b) the independence of these AGN from the environment (Silverman et al., 2009b), similar of what has been *a posteriori* found for star forming galaxies and c) the number of optical AGN with radio emission, which is negligible with respect to that of star forming galaxies.

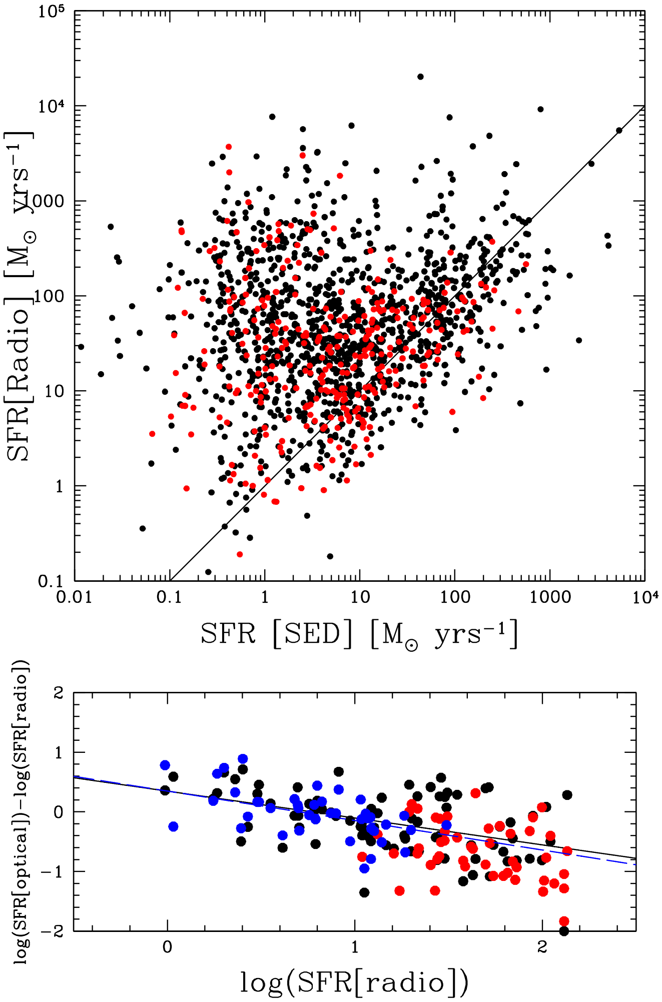

Fig. 1. Upper panel: SFR(radio) versus SFR(SED) for all radio galaxies in the initial VLA-COSMOS sample with $I < 22.5$ (black circles). In red the 315 objects within the zCOSMOS survey are highlighted. The solid black line is the SFR(SED)=SFR(radio) line drawn for reference. Lower Panel: Ratio of the SFR as determined in the optical (from SED and lines) and the SFR estimated from radio luminosity for a sample of ”bona fide” star forming galaxies (see text). In red the SFRs obtained from the [OII] line, while in blue from the Hα line. Black points refer to SFRs determined from SED. Blue and black lines are the least squares fits to line and SED determination.

3.1. AGN versus star formation radio emission

There are several recipes for dividing the radio population into sources with emission from an AGN or from star formation (SF) (see e.g. Smolčic et al., 2008; Best et al., 2005, and references therein). They are mainy based on determining the optical properties of known radio emitting star forming galaxies and defining a limit for the emission of the AGN. In particular, the method of Best et al. (2005) separates the two classes on the basis of

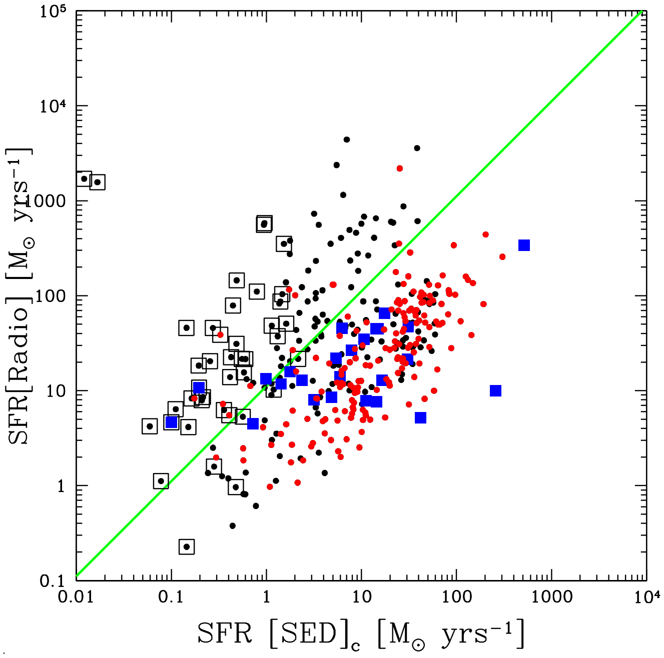

Fig. 2. SFR(radio) versus the corrected (see text) SFR(optical) for our zCOSMOS sample. Red points are star forming galaxies, blue squares are optical AGN (LINERs and Seyfert 2) as determined by line diagnostics, while empty squares are radio emitting objects in the passive region in the infrared colors-specific star formation plane (see Section 3.2). The green line is the adopted division between star forming galaxies and AGN. Small black points are objects without spectral diagnostic classification (due to low quality line measurements).

the $D_n(4000)$-$L_{1.4GHz}/M_{star}$ plane. In practice, this method compares the ages of stars (estimated with the $D_n(4000)$ parameter) with the current specific star formation rate (estimated with $L_{1.4GHz}/M_{star}$) and the chosen separation line is 0.225 above the $D_n(4000)$ value of a 3 Gyr exponentially decaying star formation galaxy track. The method of Smolčic et al. (2008) is based on the fact that the two families define two peaks in a PCA-based rest-frame colors combination. Both methods have been calibrated with the use of line diagnostics.

Our method instead has two steps. First, we compare the star formation rates estimated from the radio emission and from the spectral energy distribution fit (Bolzonella et al., 2009) and we separate AGN from SF radio sources on the basis of this comparison. For the estimate of the star formation rate from the radio emission we used the Bell (2003) formula. Second, we study the optical and infrared properties of the radio galaxies to define control samples with similar properties.

Note that our results do not depend strongly on the specific formula adopted in converting L_{radio} to SFR because our method is based on a relative comparison, which considers as AGN all objects outside a given radio-optical star formation correlation. With the zCOSMOS spectra we could also use the star formation rates derived from the lines, but we decided to use the SED determinations because: a) at low redshifts ($z < 0.5$) the emission line estimate would use the Hα line (which is affected by problems with sky line contamination and strong fringing in the spectra in the redshift range [0.3-0.5]), while at higher redshift the usable line is [OII] and b) for weak star formations the line measurements are able to provide only upper limits. We note that because of point a), the SFR estimate would not be homogeneous being based on two different lines in two different redshift ranges. Moreover, by considering only detected lines, the final usable sample would be ~ 60% of that we have with SED determinations. For this reason, we will use the spectral features only to calibrate the method.

In Figure 1 (upper panel) we show the SFR(radio)-SFR(SED) plane for the entire VLA-COSMOS sample limited to $I < 22.5$) and its zCOSMOS subsample (red points). Only in this case, used for illustratory purpose, we used the photometric redshifts as derived by Ilbert et al. (2009) both for computing distances and SEDs.

It is clear that at high ($> 10 M_\odot$ yr^{-1}) values of SFR(SED), the two quantities are reasonably correlated, defining a "star forming galaxy line", while at low values (SFR(SED)$< 2 M_\odot$ yr^{-1}) a significant population of radio sources with a radio star formation "excess" is present. This excess means that the radio emission of this population is not driven by star formation and thus is due to AGN.

However, we need to test the robustness of the SED star formation rate determination. By taking advantage of having the zCOSMOS spectra, we can apply standard line diagnostics (Baldwin Phillips & Terlevich, 1981) to classify emission line galaxies as star forming, Seyfert 2 or LINERS. This procedure was applied in an automated way to the zCOSMOS sample (Bongiorno et al., 2009) following the method of Lamareille et al. (2009). At low redshifts ($0.15 < z < 0.45$) the [OIII]/Hβ versus [NII]/Hα ratios have been used (red diagnostics), while at higher redshift ($0.5 < z < 0.93$) the objects have been classified using the line ratios [OIII]/Hβ vs [OII]/Hβ (blue diagnostics).

From the 133 radio detected galaxies classified as star forming, we selected a subsample of 83 "bona fide star forming galaxies", i.e. classified as SF galaxies from diagnostics and with high quality line measurements and with emission lines far from sky and fringing lines. In Figure 1 (lower panel) we plot the ratios of the SED (black points) or lines (red and blue points) SFR to the radio SFR determination versus the radio SFR. Red points correspond to SFR obtained from the [OII] line and blue points from the Hα line (Moustakas Kennicutt & Tremonti., 2005). Note that SED and emission line determined SFR are consistent with each other, but their ratios with the radio SFR shows a significant decrease with increasing SFR(radio).

In particular, assuming that the values of the radio SFR represent the true ones, the SFR derived from SED and emission lines overestimate the low and underestimate the high SFR. We note that the underestimate of the SFR from the Hα line (red points) for SFR $> 1 M_\odot$ yr^{-1} is qualitatively similar to the result of Caputi et al. (2008), found by comparing this estimation with the value derived from the combined UV and IR luminosity (see their figure 8).

We fitted the points in the figure (the "bona fide star forming galaxies") with a linear relation finding that $< log(\mathrm{SFR[SED]}) >= 0.55 \log(\mathrm{SFR[Radio]}) + 0.347$, where $< log(\mathrm{SFR[SED]}) >$ is the mean value of log(SFR[SED]) at a given log(SFR[Radio]). Then, we computed the "corrected" SFR[SED]$_c$ by applying the relation

$$log(\mathrm{SFR[SED]_c}) = \log(\mathrm{SFR[SED]}) - < \log(\mathrm{SFR[SED]}) > + log(\mathrm{SFR[Radio]})$$

. In practice, we force the two estimates of SFR for the "bona fide star forming galaxies" to statistically follow the relation $log(\mathrm{SFR[SED]_c}) = \log(\mathrm{SFR[Radio]})$ The r.m.s. dispersion around the fit is ~ 0.35.

Finally, we define the division line between SF galaxies and AGN to be the line parallel to the *log*(SFR[SED]$_c$) = log(SFR[Radio]) relation and shifted horizontally by 3 sigma. In this way, to be included in our AGN sample, the radio emission from the black hole should be about an order of magnitude higher than the average emission due to star formation.

Obviously, this division line between star formation and AGN is somehow subjective, because it is likely that there is some AGN contribution to the radio flux also in objects below the division line. However, this procedure ensures that we define a "clean", even if not complete, AGN sample. In particular, at higher star formations rates, we cut progressively at higher radio luminosities.

Applying this procedure we define a sample of 97 of AGN out of our total sample of 315 radio sources (Figure 2).

Among the 133 automatically diagnosed star forming galaxies, only 13 are in the AGN region. After visual checks of the spectra, we conclude that all but two could be considered incorrect or at least uncertain classifications because of a low signal-to-noise of the lines or contamination by the sky/fringing lines. This shows that a large fraction ($> 90\%$) of the objects classified as star forming galaxies on the basis of the optical spectral diagnostics are indeed recognized as such by our method.

As expected, the situation for optically classified AGN is less clear: among the 14 LINERs and 11 Seyfert 2 objects, the galaxies showing "star formation excess" are 2 and 3, respectively. Assuming that for our optical AGN the average contribution of the AGN to the line luminosity is $\sim 50\%$ (see figure 6 of Silverman et al., 2009a) and comparing the expected radio star formation from the optical-radio star formation correlation with the observed radio luminosity, we conclude that, on average, the AGN radio luminosity for these objects is a factor $\sim 3-4$ higher than that due to star formation.

Note that although the SFR(optical)-SFR(radio) plot is useful for distinguishing AGN from star forming galaxies, it can not be used to extract a consistent control sample, because the division between galaxy classes is not derived using optical properties only.

3.2. The color-specific star formation plane

We now discuss the relation between the infrared color 8.0-4.5 μm obtained by the Spitzer satellite (Sanders et al., 2007) and the optical specific star formation rate (SSFR). It is already known that near infrared colors are a powerful method for finding broad line AGN (see e.g., Lacy et al., 2004), but here we are more interested in the behaviour of the "normal" galaxy population. We define the infrared color as ratio of the two fluxes $S_{8.0}/S_{4.5}$

In the upper panel of Figure 3 we show the distribution of the galaxies of the statistical sample (as defined in Section 2), where the star forming galaxies are indicated in red, the Seyfert 2 galaxies in green and the LINER galaxies in blue, all classified with spectroscopic diagnostics. Note a number of non-classified objects (black points) that reside in the star forming galaxies, where the emission lines are expected to be strong. These classification failures can be explained by noting that the redshift distribution of these objects has two peaks at $z \sim 0.5$ and $z \sim 0.85$. In the first case, we are at the point in which the Hα line is at the red border of the observed spectrum and affected by fringing, and the [OII] line starts to enter from the blue border. At the peak at high redshift, the Hβ starts to be affected by fringing.

The existence of two populations is rather obvious and is related to the bimodality found also in the optical by using B-I or U-B colors (see Cucciati et al., 2009) for dividing red, passive galaxies from the star forming ones.

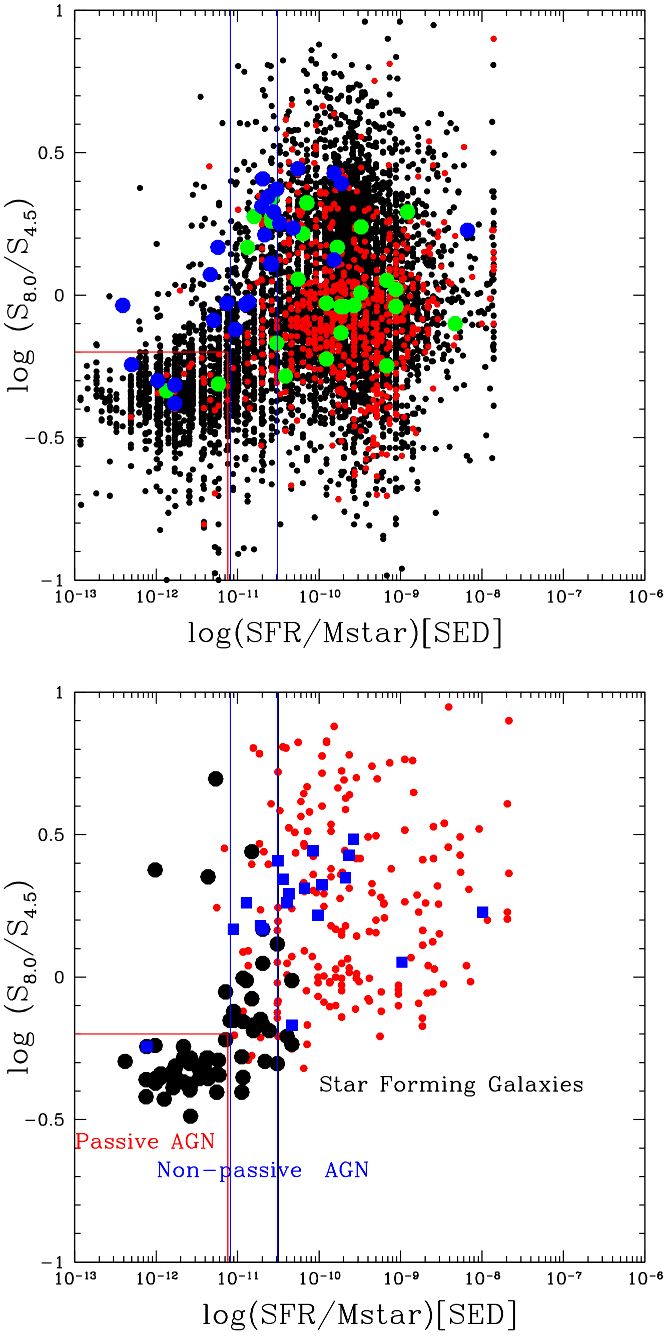

Fig. 3. Upper panel: infrared color versus specific star formation rate for all galaxies in the statistical sample. Red points represent the star forming galaxies, blue points the LINERS and green points the Seyfert 2 objects classified by line diagnostics. Black points represent unclassified galaxies (see text). Lower panel: same as the upper panel, showing only the radio galaxies. The large circles represent our defined radio AGN. Blue squares are the optical AGN (not divided into LINERs and Seyfert 2). Vertical and horizontal lines represent the division between the three galaxy populations defined in the text.

Interestingly, the Seyfert 2 objects occupy the same locus of star forming galaxies, while LINERs are at the upper border (see also figure 19 of Smolčic et al., 2008).

Passive galaxies are located in a clump in the lower left of the plot, while the star forming galaxy region has a vertex nearby the passive clump and opens at larger distance. The division value has been chosen as the point in SSFR which show a minimum in the density distribution of the galaxies.

In the lower panel of Figure 3, we show the same plot but only for radio sources. The large black circles are the radio AGN objects defined in the previous subsection.

This plot shows that the radio AGN sample consists of two different populations, one corresponding to the passive galaxies ($log(S_{8.0}/S_{4.5}) < -0.2$ and $log(SFR/Mstar) < -11.1$) and one extending toward the SF galaxies locus.

Moreover, it also appears as if there is a specific star formation limit (at log(SFR/Mstar) ~ -10.5), such that the radio AGN are rare for SSFR higher than this limit. The division at $log(SFR/Mstar) \sim -10.5$ is certainly subjective and may depends on the characteristics of the survey, but it is a fact that the majority of radio AGN are on the left of the line and are not spread throughout the plot. This division value has been chosen to maximize the number of radio AGN and minimize the contamination from SF galaxies in the region defined for AGN.

Of the 75 AGN radio sources with measured infrared color, 38 are passive galaxies, while the remainig are in the second region defined above. We note that this behaviour is similar to that shown in figure 10 of Smolčic et al. (2008) using the 8.0-4.5 μm and 5.8-3.6 μm color plane.

In Figure 2, there are a number of radio sources defined as passive which are not in the passive AGN sample, because they are not radio luminous enough to satisfy our cut. Assuming the extreme hypothesis that all these objects are passive AGN, this would mean an incompleteness of our sample of $\sim$ 15%. Recomputing all quantities with the inclusion of these objects, the following results do not change.

As a general conclusion, we define as radio AGN all objects with ”radio star formation excess”, while ”passive AGN” occupy the passive (i.e. very low specific star formation) galaxies peak of Figure 3. The remaining AGN are defined as ”non-passive AGN”, while all other radio sources are considered to be star forming galaxies.

As outlined above, this choice is justified in the light of the analysis of the environmental dependencies. It is worth emphasizing that a more sophisticated method to separate AGN from starforming galaxies, when both phenomena are present, is still lacking in the literature. Our method leads to a contamination of the star forming galaxy sample by AGN of $\sim$ 8% (after having applied the limits of Table 1). We checked that this contamination has no effect in the following conclusions.

Therefore, the control sample will be extracted using the limits taken from Figure 3 and reported in Table 1. The only exception is the additional cut that we applied to the stellar mass in the passive AGN sample, which is discussed in Section 4.2.

3.3. Comparison with other classifications

To check the consistency between our method for classifiying AGN and SF galaxies and other methods present in the literature, we will consider the spectroscopic line diagnostics (Baldwin Phillips & Terlevich, 1981), the $D_n(4000)$-$L_{1.4GHz}/M_{star}$ plane of Best et al. (2005) and the Smolčic et al. (2008) method. In Figure 4, we present a plot of the equivalent width of the [OIII]/Hβ versus [NII]/Hα (red diagnostics) and the [OIII]/Hβ versus [OII]/Hβ (blue diagnostics) line diagnostics for radio SF galaxies as defined by our method. We remind that the two diagnostics were applied to two redshift ranges ([0.15-0.45] and [0.5-0.93], respectively). Circles are objects for which all emission lines were detected. Here, an upper or lower limit implies that for each line ratio one line has been detected and for the other we have an upper limit. When we have upper limits for both lines, no point is shown in the diagram.

In the upper panel, the solid line is the theoretical Kewley et al. (2001) division between SF galaxies and AGN, while the dashed line is the Kauffmann et al. (2003) line. The region between the Kewley et al. (2001) and the Kauffmann et al. (2003) lines defines a region of so-called ‘”composite galaxies”. In the lower panel, the division proposed by Lamareille et al. (2004) is plotted as solid line and dashed lines represent the $+/-0.15$ dex uncertaintes in the classification.

Of the 100 SF galaxies within the redshift range useful for the red diagnostics, 81 have spectra with all four lines detected, while for the blue diagnostics the ratio is 63/91. As expected from Figure 2, a not negligible number (14) of the optical AGN (i.e. those defined by line ratios) are in the SF galaxy sample.

For the red diagnostics, 18 objects fall in the ”composite galaxy region”: by applying the same procedure defined in Sect. 3.1 to estimate the relative contributions of AGN and star formation rate to the radio flux, for these objects we obtained on average $\sim$ 2.5. For the non-passive and passive AGN samples, the diagnostics are inconclusive, because of the lack of detected lines for estimating the ratios. The blue and red diagnostics give a different ratio between the number of detected AGN and star forming galaxies. This is related to the different efficiency in detecting AGN of the two diagnostics, as noted in Bongiorno et al. (2009) (see their Figure 3 and 4). In particular, the blue diagnostics classify a large number of X-ray emitting AGN as star formimg galaxies, reinforcing therefore the need of new AGN-star forming division methods.

Another method for differentiating between AGN and SF galaxies through the use of the $D_n(4000)$-$L_{1.4GHz}/M_{star}$ plane (Best et al., 2005), where the age of the galaxy stellar population (estimated by $D_n(4000)$) is compared with the specific star formation rate derived from the radio luminosity. The division line adopted by Best et al. (2005) is 0.225 above the $D_n(4000)$ value of the track defined by a 3 Gyr exponentially decaying star formation. In Figure 5 we show our samples in this plane. The number of AGN below the division line is 5 (out of 104), while $\sim$ 50% of our SF galaxies are above the Best et al. (2005) dividing line and they would be classified as AGN on the basis of this criterion. These galaxies are likely in a transition region, where our AGN induced emission objects are mixed with the SF ones.

The Smolčic et al. (2008) PCA based classification is another, complementary way for classifying AGN and star forming objects. Of the 129 AGN defined in Smolčic et al. (2008) in common with the zCOSMOS sample, 66 are star forming excess galaxies in our classification scheme (and therefore AGN), while 9 out of 97 of the Smolčic et al. (2008) star forming radio galaxies are in our AGN locus. The fraction of AGN that have $log(SSFR) < -10.5$ is $\sim$ 60%. A similar percentage of star forming excess was found in the AGN sample as defined in Bardelli et al. (2009), where a spectrophotometric division is adopted. The apparently large difference between our and the Smolčic et al. (2008) method is largely due to the fact that optical AGN and composite galaxies are included in the AGN sample in Smolčic et al. (2008) and not in our scheme.

In fact, by applying our diagnostics to the Smolčic et al. (2008) sample, we confirm that the contamination of their AGN and star forming sample is $\sim$ 17% and $\sim$ 10%, respectively consistent with what is estimated in their paper.

Table 1. Sample definition: numbers in the third and fourth columns are with and without the ”evolving” magnitude limit

sample	limits	Number in radio sample	Number in Control Sample
”passive AGN”	log(SFR/Mstar)[SED]<-11.1 & log($S_{8.0}/S_{4.5}$) <-0.2	38/38	524/530
”non-passive AGN”	-11.1<log(SFR/Mstar)[SED]<-10.5	31/37	496/581
star forming galaxies	log(SFR/Mstar)[SED]>-10.5	154/186	1672/3154

A general conclusion of this comparison is that our approach, which entirely relies on the comparison of observed radio power with the expected power due to the star formation, is more conservative (and therefore not complete) in selecting radio AGN than other methods. We remind that our method was constructed to classify as AGN those objects for which the radio flux is dominated by the central engine.

4. Differences between radio loud and control samples

4.1. Spectral differences between radio loud and control samples

The most basic approach is to construct composite spectra of the samples.

In Figures 6 and 7, we show the composite spectra for the passive, non-passive radio AGN and star forming galaxies and their control samples. Moreover, we plot the difference between the radio and control sample composite spectra.

For passive AGN, there is no significant difference between the composite spectra of the radio loud and control sample, implying that there is no obvious AGN signature in their optical spectra. There is only an indication for radio spectra to be redder than the control sample.

The spectra of both the non-passive AGN and control sample objects exhibit significant [OII] emission lines, as well as absorption lines (like H+K Ca and Mg 5175 Å) and relatively weak [OIII] and $H\alpha$ lines.

In both spectra Hβ is in absorption only. All these spectral features imply that these galaxies are of relative early type. All galaxies from the non-passive AGN and control sample are indeed classified by Zucca et al. (2009) as spectrophotometric type 1 and 2 (roughly corresponding to Sa-Sb). However, non-passive AGN tend to be of even earlier spectrophotometric types than the control sample. The radio sample has stronger [OII] equivalent widths (15Å versus 7Å) with respect to the control sample.

Considering the star forming galaxies, the difference between the two composite spectra is negative in [OII] and positive in $H\alpha$, implying that in radio emitting star forming galaxies a larger amount of line extinction (from dust) is present. This is confirmed by the fact that the continuum of radio emitting galaxies is redder than the control sample. This is related to the differences in colors already found by Bardelli et al. (2009) for VVDS radio galaxies and present also in our VLA-zCOSMOS sample.

Additional information about the spectral features can be derived from the equivalent width distribution of the lines. We checked this point by examining the distribution of the equivalent width of the [OII] 3727 Å line and the 4000Å break (as measured in Mignoli et al., 2009). There are no significant differences between the distributions of these quantities for passive AGN and their control sample.

Viceversa, the radio detected star forming objects have a 4000 Å break slightly shifted toward higher values than the corresponding control sample. Given that the stellar mass distribution of the radio detected star forming galaxies and control sample is different and that our data show a stellar mass- 4000 Å break relation, this difference is likely due to the different stellar masses sampled (see Section 4.2). In fact, the differences disappear considering objects with stellar mass $> 2 \times 10^{10}$ $M_\odot$, for which the mass distributions of the radio star forming galaxies and their control sample are identical (see Section 4.2).

More subtle is the difference for the non-passive AGN sample (Figure 8). In this case the radio detected objects have higher values for the 4000Å break with respect to the control sample and lower values for the equivalent width of the [OII] 3727 Å line (the probability for the KS test that the two distributions come from the same distribution is ~ 0.005).

The last question is whether the control sample of the non-passive AGN shows some sign of AGN activity in their emission lines. In Figure 9, we show the diagnostic diagrams for this sample. The blue and magenta circles correspond to the values obtained from the composite spectra of non-passive AGN and their control sample, respectively. Considering the galaxies with both all lines detected or only one line detected in the considered ratio, $\sim$ 50% of this sample consists of optical AGN or upper limits consistent with that of AGN. Note that this fraction is higher in the red, low redshift diagram. These fractions are broadly consistent with those of the radio sample, although the number of objects with all detected lines or meaningful upper limits is only 20 for the radio detected non-passive AGN sample.

We note that the points corresponding to the composite spectra are not in the middle of the distribution of the ratios of single galaxies. This is because the composite spectra are obtained also considering objects not plotted in Figure 9 (which are $\sim$ 48% and 27% of the samples in the blue and red diagram, respectively) because of the lack of detected lines. Therefore, composite spectra are not expected to have the average ratios of the plotted points.

4.2. Stellar Mass distributions

Before studying the effect of the different environments on the radio galaxies, it is necessary to verify the consistency between the stellar masses of the various samples of radio galaxies defined in the previous sections with those of their respective control samples. Given the mass-density relation (Scodeggio et al., 2009; Bolzonella et al., 2009), a difference in the stellar mass distribution may induce a difference in the observed overdensity distributions, which would not be related to AGN or star formation mechanism.

To consider a homogeneous population at all redshifts, we selected galaxies and radio sources within an optical luminosity complete, volume limited sample at $z < 0.9$. To take into account the observed optical luminosity evolution (Zucca et al., 2009), the absolute magnitude limit was defined to be $M_B = -19.8 - z$. This limit in absolute magnitude corresponds to the zCOSMOS limit in apparent magnitude ($I < 22.5$) at $z = 0.9$. In Figure 10 we show the observed mass distibution of the passive AGN and their control sample.

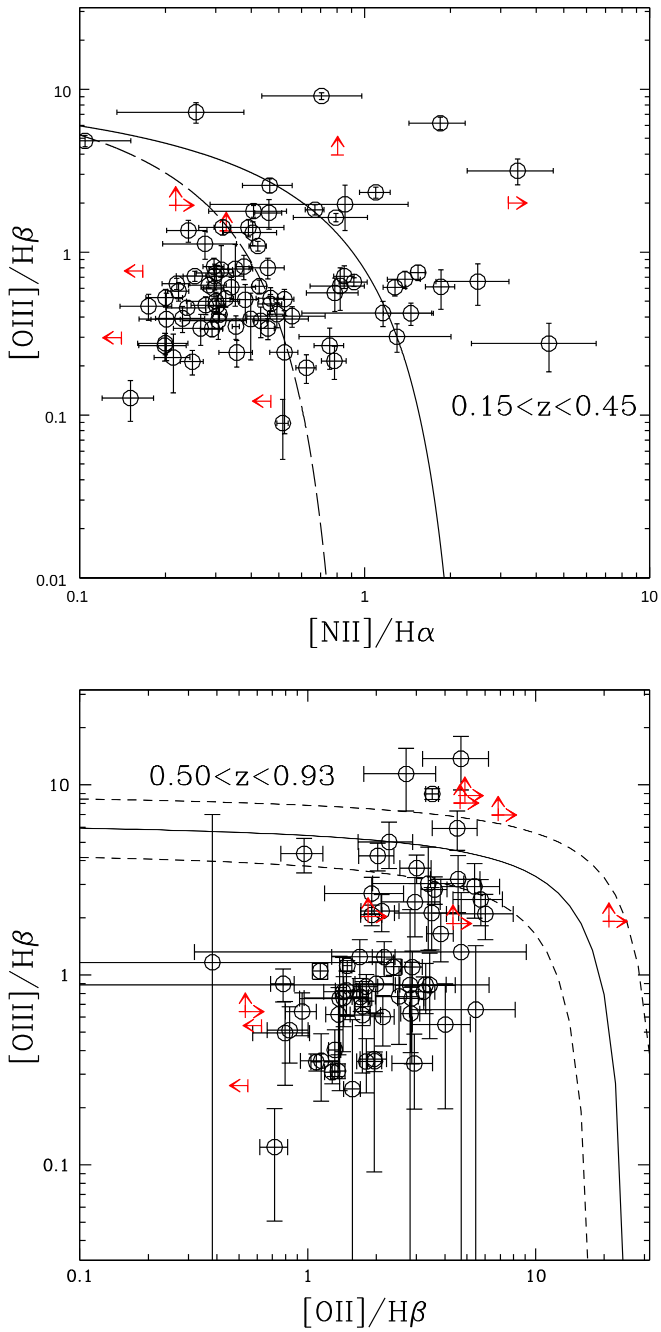

Fig. 4. Red and blue diagnostics diagram for our star forming galaxies with radio detection. Circles are objects with all lines detected. For the upper or lower limits, we plot only objects with only one upper limit determination for each line ratio.

For the control sample, since we have a volume limited sample, we plot the stellar mass histogram. Since the mass completeness limit is changing with redshift (from $\sim 10^9 M_\odot$ at $z \sim 0.3$ to $\sim 5\ 10^{10} M_\odot$ at $z \sim 0.9$)(see Pozzetti et al., 2009), our observed stellar mass distribution shows an increasing incompleteness at decreasing stellar mass. Assuming that the incompleteness is the same for the control sample and the radio sample, only the relative comparison between the control and radio sample is relevant here. The radio sample, which also has the limit in radio flux in addition to the limit in apparent magnitude, needs to be corrected for V_{max}.

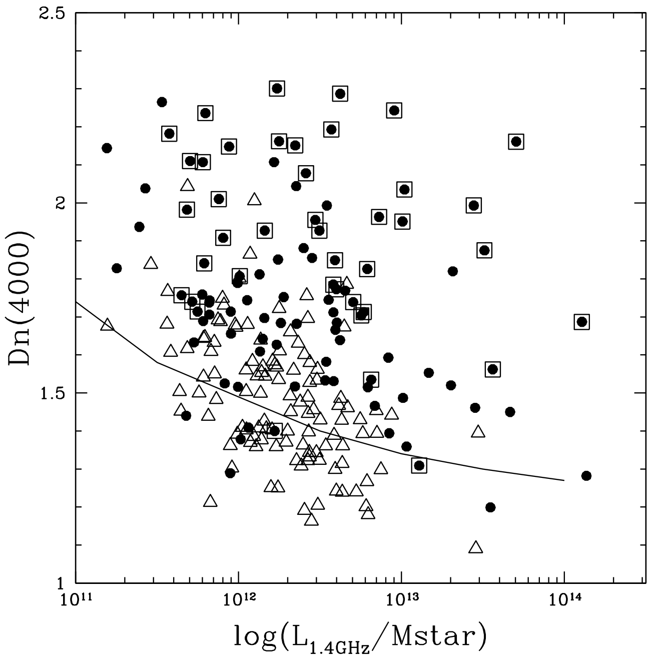

Fig. 5. Dn(4000) versus $L_{1.4GHz}$/Mstar plane: Triangles are our star forming galaxies and circles our AGN sample. Open squares indicate the passive AGN.

The first result is that all radio emitting objects have $log(Mstar) > 10.7$, while the control sample has a broader mass distribution. For this reason, in the following analysis we limit the control sample to $log(Mstar) > 10.7$.

We note that the ratio of the stellar mass distribution of radio emitting passive AGN to its control sample is rather constant at $\sim$ 20%. This is apparently inconsistent with the results of Smolčic et al. (2009a), for which the ratio of radio AGN to the control sample is rapidly increasing with stellar mass. The difference could be understood considering that we study only a specific class of AGN and apply a significantly high cut in absolute magnitude to create a volume limited sample at the depth of zCOSMOS. On the other hand, Smolčic et al. (2009a) considered volume limited samples in terms of the radio limit (i.e. fixing a limit in the radio luminosity) and corrected for V_{max} the optical incompleteness. Their apparent magnitude (and consequently absolute magnitude range) limit is deeper than that of zCOSMOS survey. In fact, considering all AGN (passive+blue) and avoiding the absolute magnitude limit, we derive similar ratios as Smolčic et al. (2009a).

For non-passive AGN the ratio of the two stellar mass distributions (radio detected and control sample) is $\sim$ 5% for masses $< 10^{11}$ $M_\odot$ (see upper panel of Figure 11), while at higher masses the ratio is $>$ 25% We note that in this case we recovered the mass dependence of the AGN activity.

For star forming galaxies, the lower panel of Figure 11 indicates that the the two stellar masses distributions are the same for masses higher than 2×10^{10} $M_\odot$ and differ for lower masses, consistent with a similar plot in Bardelli et al. (2009).

We interpret this trend as implying that the stellar mass distribution of radio detected star forming galaxies is the convolution of the stellar mass function of these objects with the star formation rate distribution at fixed stellar mass or absolute magnitude (see Bardelli et al., 2009). The mean star formation rate increases with mass, but the distribution has significant tails. At

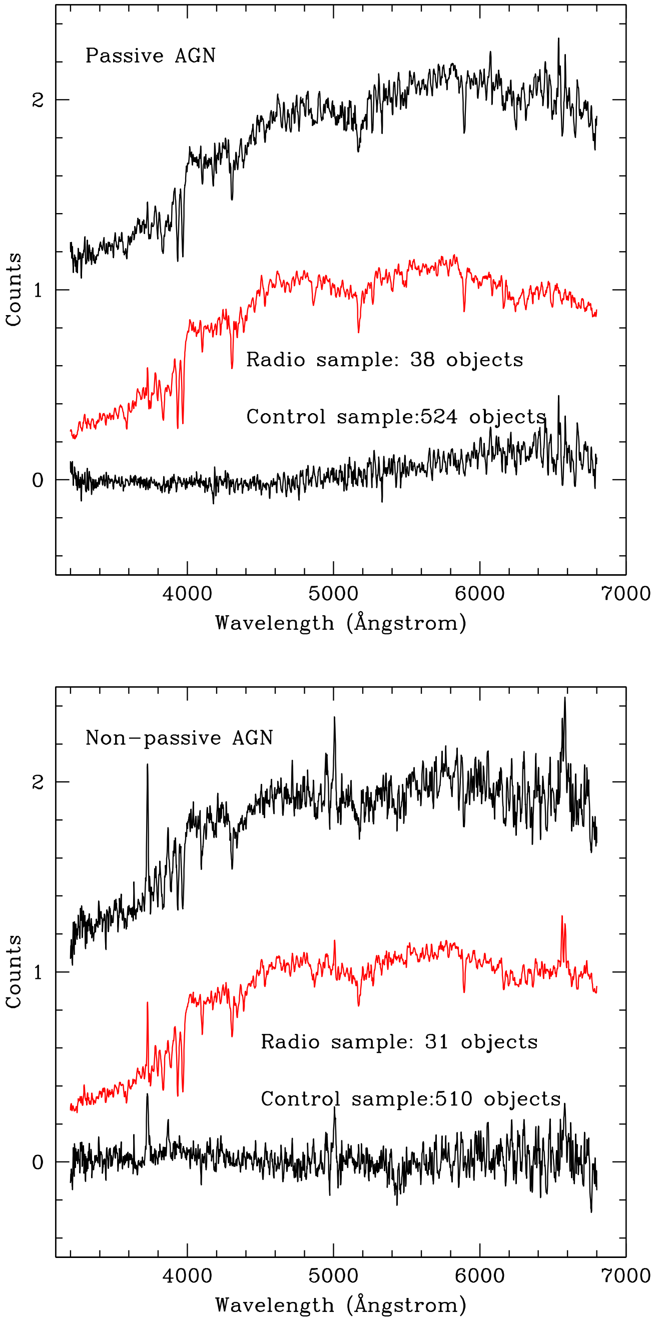

Fig. 6. Composite spectra for the radio emitting AGN (in black, upper spectrum) and the control sample (in red, middle spectrum). The upper panel refers to passive AGN and the lower panel to non-passive AGN. The spectrum of radio sources is shifted for clarity by 0.9 in the y-axis. At the bottom of the figures, we plot the difference between radio emitting objects and control sample (lower spectrum).

lower stellar massses an increasing number of objects with star formation rate in the low tail is below the flux limit of the radio survey. More specifically, the lower limit for the star formation rate is set to $log(\mathrm{SFR/Mstar}) \sim -10.5$ from Figure 3, which corresponds for $log(Mstar) = 10.3$ (the "completeness limit") to $\sim 0.6 M_{\odot}\ \mathrm{yr}^{-1}$, similar to the minimum observed star formation rate. For lower masses the limit is lower than the minimum observed star formation rate.

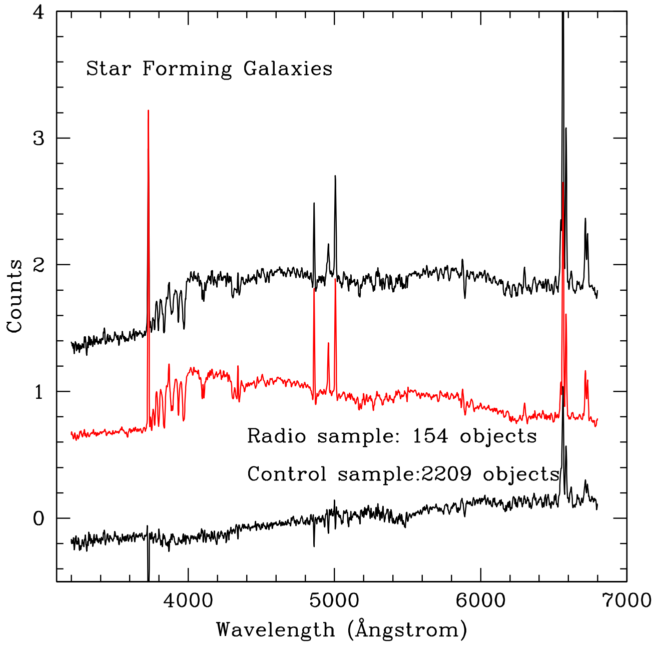

Fig. 7. Same as Figure 6 but for the radio emitting star forming sample and its control sample.

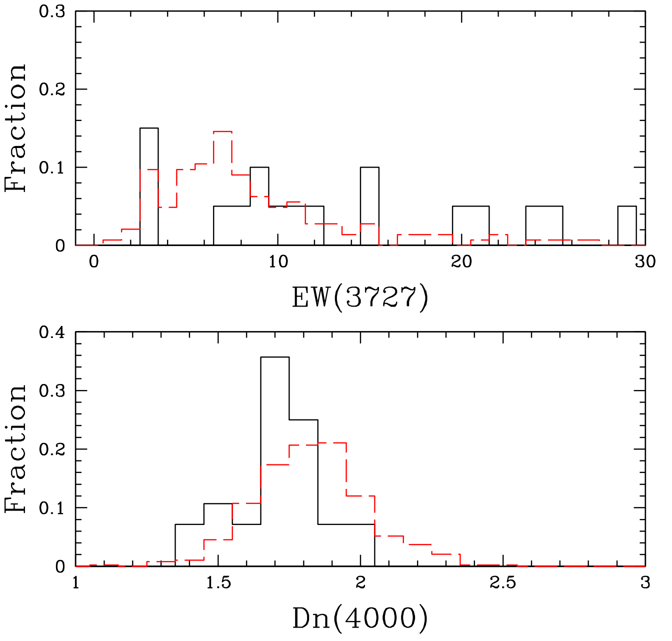

Fig. 8. Equivalent width and Dn(4000) distributions for the radio and control sample for the non-passive AGN. The dashed red line is for the control sample and the black solid line is for the radio sample.

For the density analysis we limit the control sample to $log(Mstar) = 9.7$ for the star forming galaxies and to $log(Mstar) = 10.4$ for non-passive AGN. These limits correspond to the minimum mass detected in the radio samples.

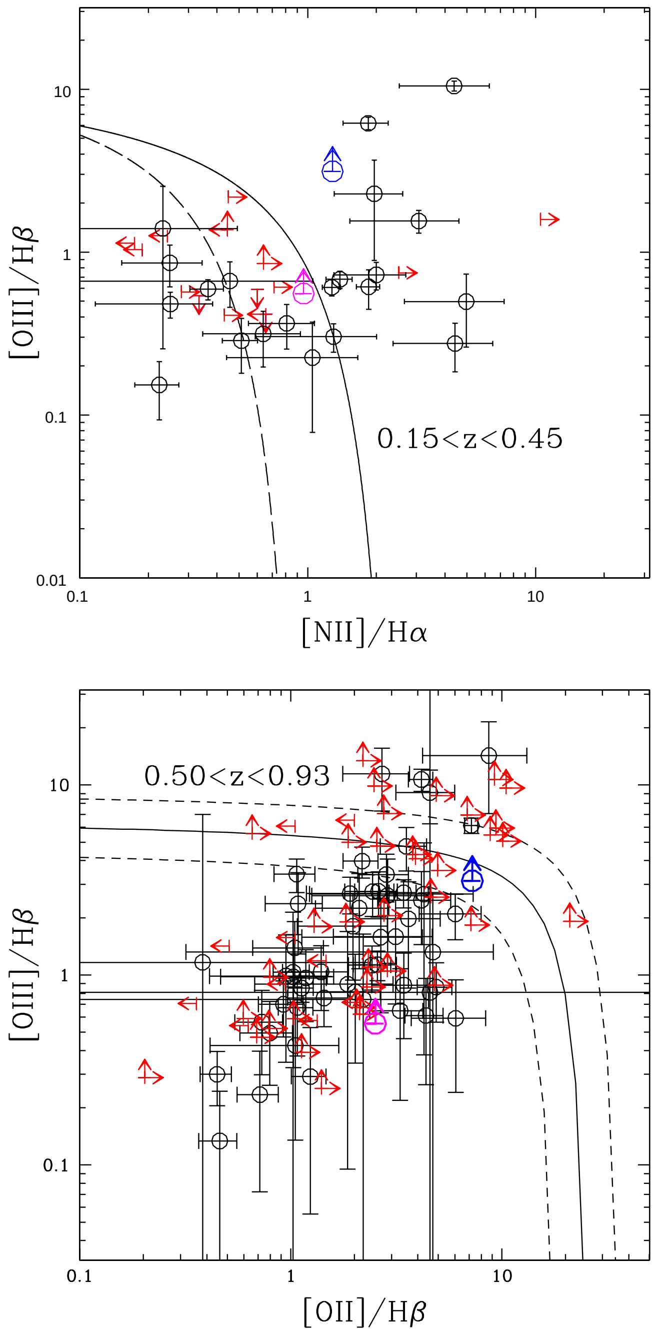

Fig. 9. Line diagnostics for the control sample of the non-passive AGN sample. The blue and magenta points correspond to the values obtained from the composite spectra of non-passive AGN and control sample respectively.

5. Environmental effects

5.1. Method

To consistently define our radio and control sample we adopted the limits reported in Table 1. We computed the density distributions by considering all objects with $z < 0.9$ and brighter than an ”evolving” absolute magnitde limit $M_B < -19.8 - z$, where z is the galaxy redshift. This evolving limit was introduced in order to take roughly into account the luminosity evolution of the galaxies as determined from the luminosity function estimate by Zucca et al. (2009, 2006) and therefore to approximately consider the same population at all redshifts. Moreover, in the case of the passive AGN sample, we also applied a cut in stellar mass at $log(Mstar) > 10.7$, for the non-passive at $log(Mstar) > 10.4$ and for the star forming galaxies at $log(Mstar) > 9.7$ (see Section 4.2).

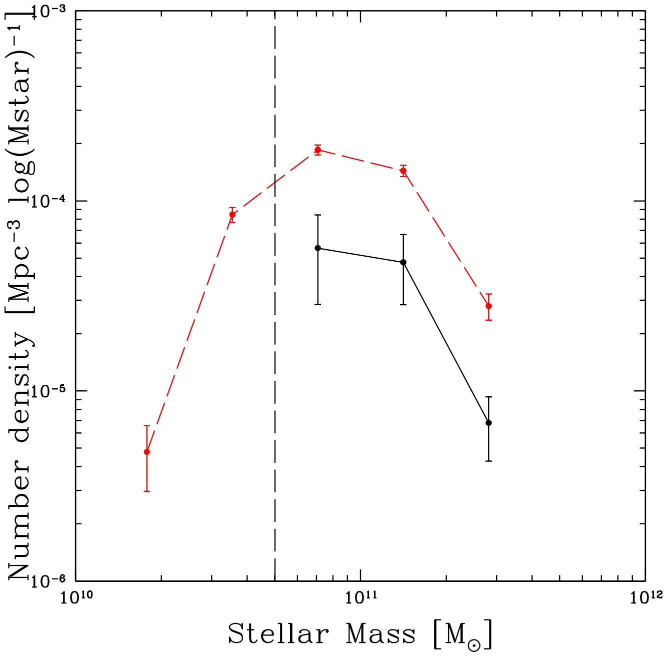

Fig. 10. Stellar mass distribution of the passive AGN (black continous line) compared with its control sample (red dashed line). The vertical dashed line indicates the adopted stellar mass cut.

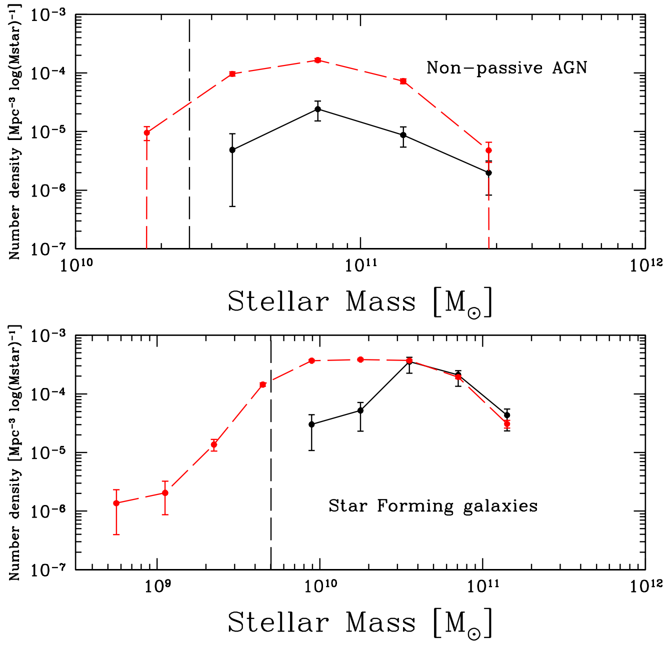

Fig. 11. Upper panel: Stellar mass distribution of the non-passive AGN (black continous line) compared with its control sample (red dashed line). Lower Panel: same but for star forming galaxies.

5.2. Redshift distribution

The most basic approach to assess a possible dependence of radio galaxies on the environment is to compare their redshift histogram with that of the control sample. In Figure 12 (upper and lower panels) the normalized histograms of the radio sources (solid black line) and of the control sample (dashed red line) are shown.

In this figure, we cut the radio sample at $\log L_{Radio}$ (W Hz^{-1})> 23 to obtain a volume limited sample also in terms of radio luminosity. Variations in the ratio of the number of radio galaxies to those in the control sample found in correspondence to peaks or valleys of the galaxy distribution would indicate a different environment distribution between the two populations. Smoother variations as a function of redshift would imply an evolution of sources.

In the upper panel we consider all AGN (non-passive + passive), i.e. those radio sources with star formation rate excess and, for the control sample, all galaxies with $log(SSFR)(optical) < -10.5$. In the middle panel, we show the ratio of the two histograms in order to visualize better any redshift dependence. Errors are presented at the 1 σ confidence level. Black points correspond to the whole AGN sample, while red points refer to passive AGN. For clarity the red points have been shifted by +0.03 along the x axis.

In the lower panel we show the redshift distribution of star forming galaxies.

The number ratios of both AGN and SF radio samples to the respective control samples are rather constant. This implies that the radio samples follow the same large scale distribution as the control samples and therefore no large segregation with the density is present at the largest scales. For the two classes of AGN taken separately, the ratio values are around 0.07 for the non-passive AGN sample and 0.06 for the passive AGN sample.

The redshift histograms explore densities which are on the largest scale possible for our redshift survey, ranging from ∼ 12 Mpc at $z \sim 0.3$ to ∼ 21 Mpc at ∼ 0.5. In the following, we explore smaller scales using the 5^{th} nearest neighbor.

5.3. The nearest neighbour determined overdensity distribution

We used the densities estimated from the distance of the 5^{th} nearest neighbour (Kovač et al., 2009) and the volume limited sample as tracer of the density field. In this case, the tracers are the galaxies with absolute B band magnitude brighter than $-19.5 - z$ up to redshift 0.7, while for redshifts between 0.7 and 1, the tracers are galaxies with $M_B < -20.5 - z$. This corresponds to overdensities computed on average scales of ∼ 2.4 Mpc, thus not much larger than the typical extent of a cluster. We also checked the results for the other tracers described in Kovač et al. (2009), but the results did not change. Among the various available weighting schemes, we used the densities weighted by the stellar masses of the galaxies, but the results did not change either when using the no-weight (i.e. number weighted) estimator.

In Figure 13 we compare the overdensity distribution of the three radio samples (black solid histograms) with those of their respective control samples. In the upper left panel, we present the total AGN sample. We recall that in this case the radio sample comprises all radio sources with star formation excess and the control sample comprises all objects with $log(SSFR)(optical) < -10.5$. The two distributions are different at about 2σ level on the basis of the K-S test.

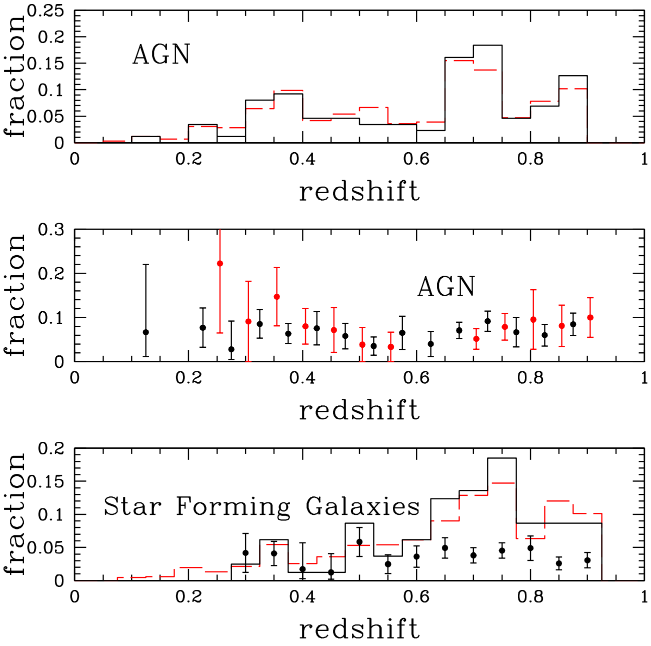

Fig. 12. Upper and lower panels: fractional redshift distributions of our samples. Red dashed histogram: control sample. Black solid histogram: radio sample. Histograms have been normalized to the number of objects. Upper Panel: AGN sample (passive+non-passive). In the middle panel, we show the ratio between the number of radio AGN and the control sample. Red points represent the fraction of radio loud passive AGN (shifted for clarity by 0.03 in the x axis). Lower panel: Star forming galaxies redshift histograms and relative ratios (black points).

A much stronger statistical signal of difference (as evaluated by the -KS test probability) is obtained by considering only the passive AGN (upper right panel). Here, we note a lack of radio sources at low overdensities (< 3) and an excess at high overdensities (> 10). In fact, the signal present in the whole AGN sample is coming entirely from passive AGN. If we select only the non-passive AGN sample, the KS test does not find any significant difference (lower left panel). In Figure 14 we plot the same data but now as ratio of the number of radio emitting passive AGN to the control sample. As can be seen, the ratio steadily increases with the density from 0.02 to 0.2.

There is the possibility that this behaviour is caused by the fact that the *observed* ratio of the stellar mass functions of radio to the control sample shows a strong variation between 0.02 (in the bin at lower mass in Figure 10) to ∼ 0.2 (in the highest bin). Note that in Figure 10 we showed the *Vmax corrected* mass distributions. In other words, spurious density differences caused by the stellar mass-density relation could be induced both by real differences in stellar mass fucntions between radio and control samples, but also by the fact that the observed mass distributions are different (although the mass functions are similar) merely because of the flux limit.

To check this fact, we recomputed the control sample overdensity histogram of the upper right panel of Figure 13 by weighting all masses by the ratio of the observed mass distribution of the radio to that of the control sample. The results changed by a negligible amount. We checked a possible dependence with the redshift of the difference between the environments of radio and control sample. The differences between radio and control samples remain significant although the density distributions of both samples have higher density tails at lower redshift, consistent with the evolution of galaxies and of the overdensities. We conclude that no redshift evolution is present in the density-radio emission relation.

Another apparently significant difference in environment distribution between radio and control sample is coming from the star forming galaxies. The radio emitting star forming galaxies reside in systematically higher densities than the control sample. However, we note that also for star forming galaxies the stellar mass functions for the radio and control sample differ (lower panel of Figure 11).

We repeated the previous procedure to correct the control sample for the stellar mass distributions ratios and we find that the significance of the difference disappears. To do this we computed the χ^2 probability of the two distribuions: we can not use the KS test because of the binned mass ratios assumed for the correction: the probability that the two distributions are the same increases from ~ 0.05 to ~ 0.90.

Therefore, we conclude that most of the difference between the overdensity distributions of radio and control star forming galaxy samples is caused by the different stellar masses distribution sampled by radio and control samples (higher masses reside in higher densities) and not by the physical role of the environment on the radio emission.

All results showed in this paragraph are stable also using the 10^{th} and 20^{th} nearest neighbor, which correspond to scales of 3.5 and 5 Mpc, respectively.

5.4. Groups of galaxies

In Figure 15 we show the ratio of the number of radio passive AGN to the control sample as a function of group richness. The fraction of passive galaxies which are AGN in the isolated galaxies sample is 0.052 (16/307), while the fraction in groups is 0.104 (14/135), i.e. the difference is not statistically significant. It is however worth noting that 2/3 of the control sample galaxies are isolated and 1/3 are in group, while the radio passive AGN are nearly equally distributed in the two classes.

However, if we limit the group sample at richness> 4 (for which the contamination by false groups is small) the fraction of radio passive AGN becomes 0.138 and the significance of the difference between the fraction of passive AGN among isolated galaxies and in groups to 2.15σ. In fact, the overall distributions of radio and control samples has a significance derived from the K-S test of 8% to be drawn from the same distribution. Therefore, there is a small signal coming from an increase of the fraction of radio objects with richness.

6. Properties of the passive AGN

In the previous Section we showed evidence that passive AGN have an increasing probability to be a radio source in denser environments. Here, we explore if other properties of single passive AGN also change as a function of local density. In practice, we divided the sample of passive AGN in two bins at a value of $1 + \delta = 10$, and compared a number of quantities for the two sub samples. First of all we computed the two luminosity functions, We note that in our case it is only possible to consider differences in shapes, as the relative normalizations are influenced by the volume occupied by the various overdensities within the survey volume, and this is difficult to control. For this reason, we compared only the shapes which resulted to be indistinguishable.

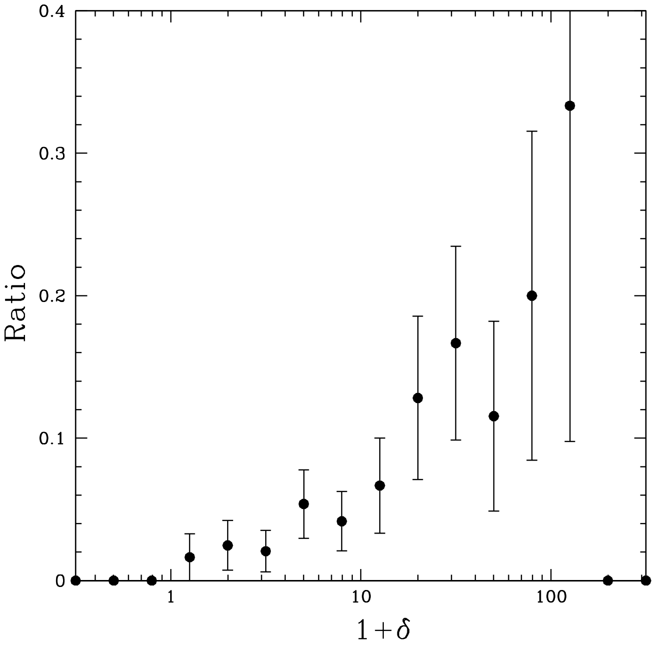

Fig. 14. Ratio between the radio and control sample of passive AGN as a function of the density.

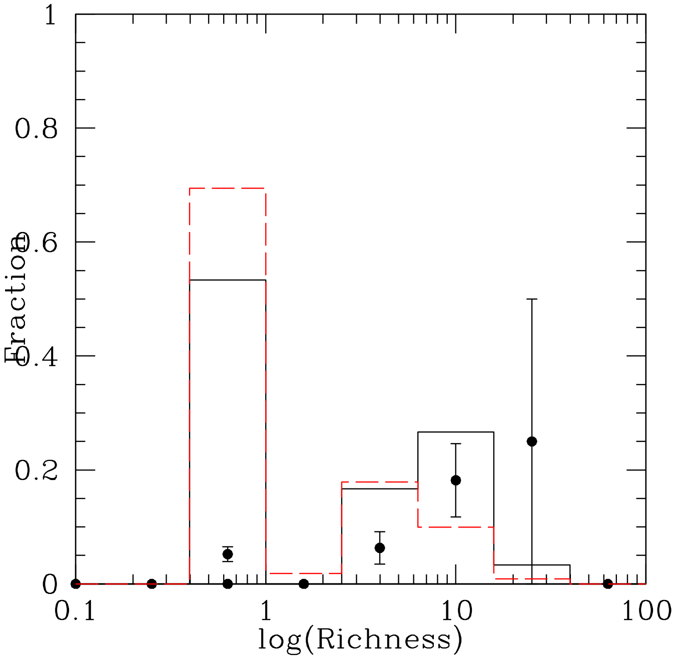

Fig. 15. Fractional distribution of richness of the groups where radio passive AGN (solid line) and galaxies of the control sample (red dashed histogram) reside. Circles with error bars represent the ratio between the numbers of objects of these two samples.

This is not unexpected because already Ledlow & Owen (1996) found that the radio and field luminosity functions have similar shape.

In Figure 16 (upper panel) the radio power-stellar mass ratio is plotted. Dashed red lines correspond to the high density sample and the solid blue line is the low density one. Each ratio has been weigthed by its V_{max} following Bardelli et al. (2009). It

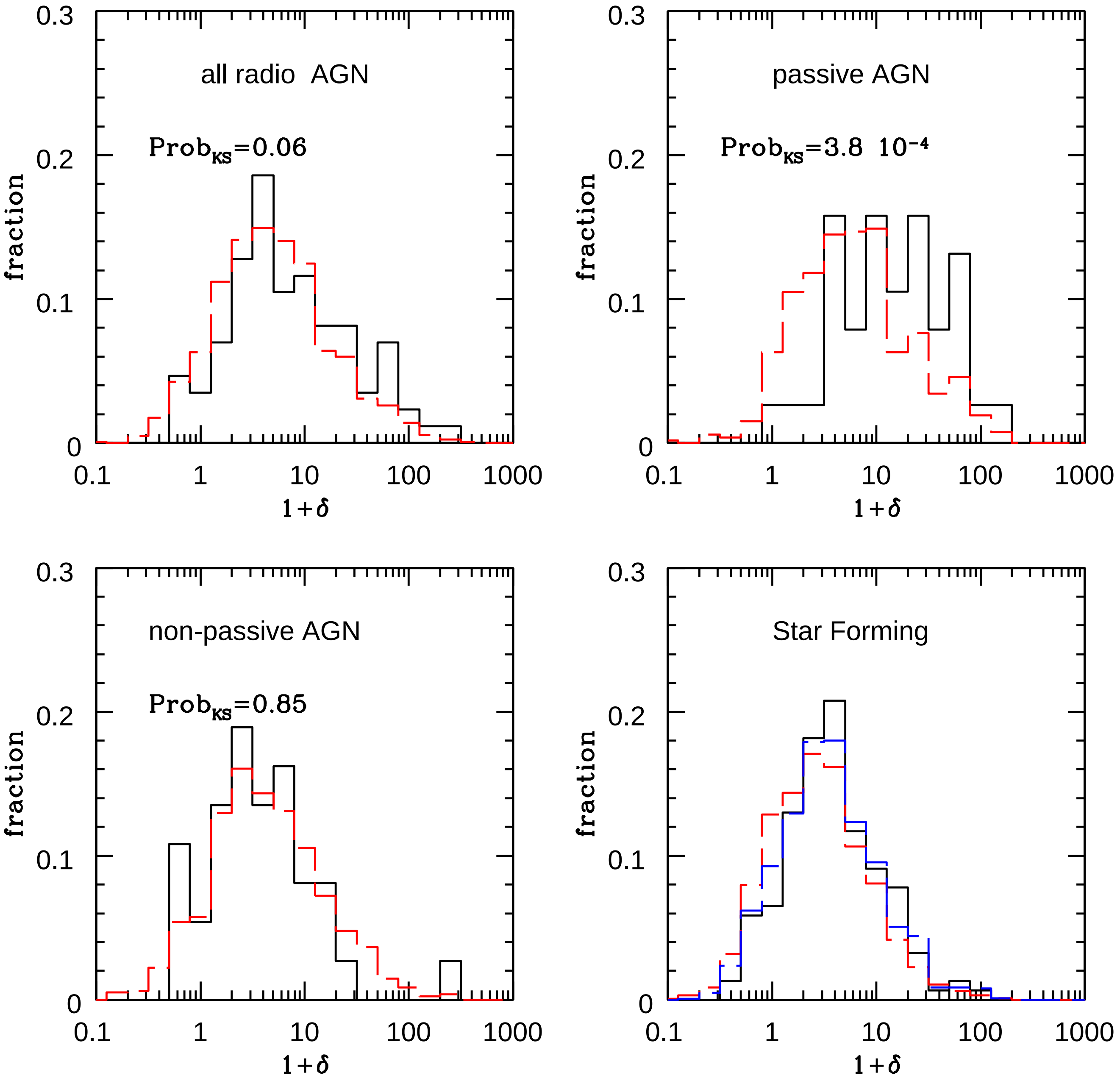

Fig. 13. Black histograms: overdensity distribution of the radio sources, Red dashed histograms: control samples. Upper left panel: total AGN sample. Upper right panel: Passive AGN sample. Lower left panel: non-passive AGN. Lower right panel: Star forming galaxies. The blue histogram corresponds to the corrected control sample.

appears that, at a given stellar mass, the radio luminosity of the AGN is significantly higher in dense environments.

In the lower panel of Figure 16, we plot the radio luminosity versus the stellar mass. We note that the difference between the two panels is that in the upper one the radio luminosity-stellar mass ratio is corrected by V_{max}, while in the lower panel we plot the observed points. It seems that there is a transition luminosity (at $\log L_{radio}$(W Hz^{-1})= 23.5), below which the objects are about equally distributed in low and high density regions, while above this luminosity ~ 80% of radio sources reside in high density regions. There is also an indication that below the luminosity threshold, a correlation between mass and luminosity is present (confirmed by a Spearman rank correlation test), which disappears at higher luminosities.

In Figure 17, we show the black hole mass distribution for the passive AGN (black) and the control sample (red). We estimated the black hole mass using the prescription of Marconi & Hunt (2003)

$$\log_{10}\left(\frac{M_{BH}}{M_\odot}\right) = 8.21 + 1.13\left[\log_{10}\left(\frac{L_K}{L_\odot}\right) - 10.9\right]$$

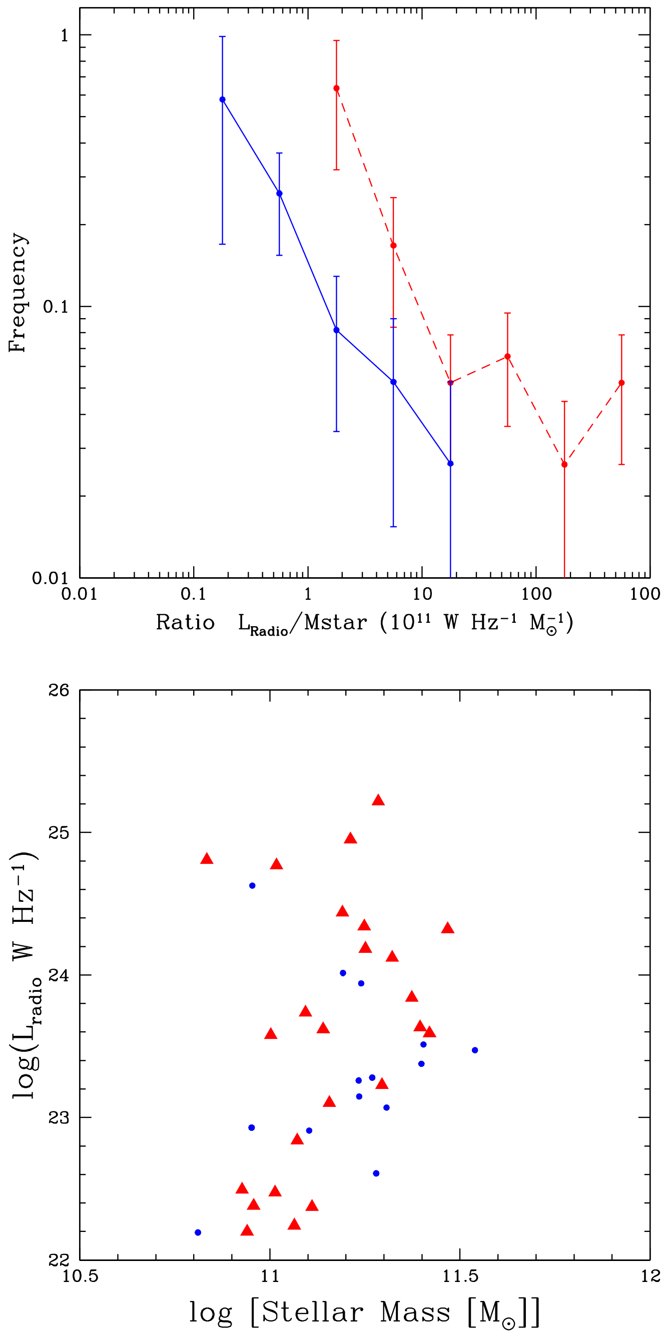

Fig. 16. Upper Panel: Distribution of L_{Radio}/Mstar for passive radio AGN in two bins of overdensity (red dashed line for high and blue continous line for low overdensity). Lower Panel: Radio luminosity versus Stellar Mass for the same samples. Red triangles represent high densities and blue points the low densities.

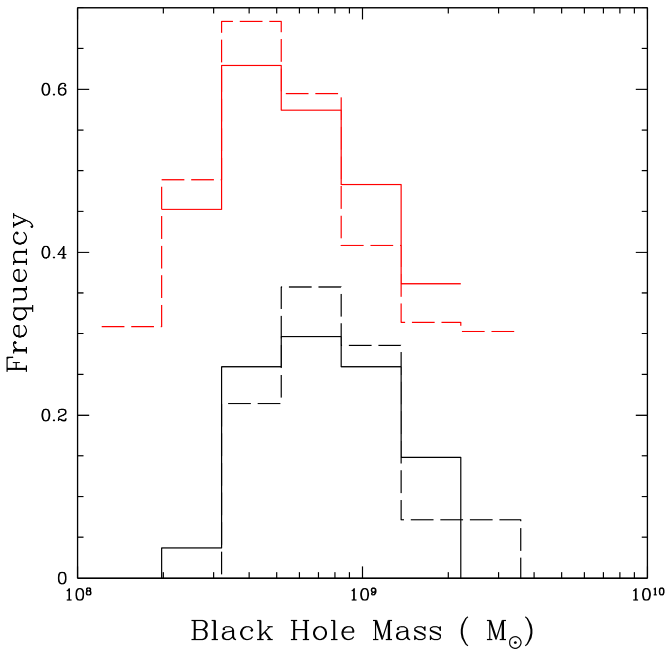

Fig. 17. Black solid histogram: high density ($1 + \delta > 10$) black hole masses distribution for passive AGN. Black dashed histogram: same distribution but for objects with ($1 + \delta < 10$). In red the distribution of masses for the control sample, shifted for clarity along the vertical axis by 0.3.

where L_K is the K-band luminosity of the galaxy. We show the results for the local M_{BH}- L_K relation, because Peng et al. (2006) claim that this relation does not change with redshift. We also corrected the Marconi & Hunt (2003) formula as done by Smolčic et al. (2009a) for the evolution in luminosity of a passive population (see Hopkins et al., 2006) but the results did not change.

There is no significant difference in the mass distribution between high and low density AGN. The only difference is between the high and low density control sample (with a KS probability for the two distribution to be equal of $\sim$ 0.005). If we plot the radio luminosity versus the black hole mass (not presented here) we obtain a plot similar to the lower panel of Figure 16 with the stellar mass substituted by the black hole mass. This is reasonable considering the relation between stellar mass and K-band luminosity.

Our general conclusion is that the main difference between passive AGN in low and high environments is a difference in radio power and that this is due, given the similarity in the black hole masses, to the host galaxies or environment structure.

7. Discussion and conclusion

Studying the environment of radio galaxies requires a division of the radio sources on the basis of their emission mechanism, because AGN and star forming galaxies may be influenced differently by the local density. To do this, we compared the star formation rate estimated from the spectral energy distribution with the one derived from the radio luminosity. We found a clear correlation between these two quantities for the star forming galaxies: we defined as AGN those objects for which the radio star formation rate is significantly higher than the optical one. In other words, these objects have a radio luminosity significantly higher than that predicted by their star formation. We assume a stringent cut at which the AGN radio emission is more than an order of magnitude higher than the star formation one in the same galaxy. In this way we excluded from our radio-based AGN sample those AGN defined on the basis of their optical emission lines, such as Seyfert 2 and LINERs, for which the ratio of AGN to star forming radio emission is lower than the adopted threshold.

Since AGN are hosted primarily by early type optical galaxies and star forming objects are basically spiral galaxies, we expect to recover at least the optical morphology-density relation (Dressler, 1980), not related to the radio emission. Therefore, to investigate whether there is an environmental effect on the radio emission, we defined control samples to be compared with the AGN and star forming radio samples. To achieve this, we studied the positions of radio sources and zCOSMOS galaxies in an infrared color-specific star formation plane. We defined three populations: passive AGN, non-passive AGN and star forming galaxies. The passive and non-passive division is reminescent of the low and high-excitacion dichotomy described in Smolčic (2009) and probably corresponds to two different processes of accretion (hot and cold, respectively). In fact, the two processes are expected to depend differently on the environment (Hardcastle Evans & Croston, 2007). The radio luminosity functions of the passive and non-passive AGN are similar in shape but not in luminosity range. Non-passive AGN stop at $\log L_{radio}(\mathrm{W\,Hz^{-1}})= 23.4$, while the passive AGN reach $\log L_{radio}(\mathrm{W\,Hz^{-1}})= 25.2$.

Finally, our radio objects belongs almost all to the FR-I class (as defined by Ledlow & Owen, 1996) and the sample lack of the broad line AGN class. Therefore we focussed mainly to objects triggered by gas accretion and did not considered other mechanism as e.g. mergers.

Passive AGN: This population of AGN is hosted by red galaxies. Using the morphological classification derived from HST/ACS images through the ZEST algorithm (Scarlata et al., 2007; Tasca et al., 2009), we find that $\sim$ 85% of both passive AGN and relative control sample are classified as early type (i.e. bulge dominated). The spectra of these galaxies with and without radio emission are indistinguishable and the ratio of their stellar mass functions is rather constant at ~ 0.2 for masses higher than 5×10^{10} $M_\odot$. This value can be interpreted as corresponding to the average fraction of time during which the central engine is switched on. Note that our ratio is derived comparing the mass functions: if we had used the observed number of galaxies, we would have found values more similar to those reported in Table 4 of Shabala et al. (2008) (~ 0.5 at high masses, ~ 0.15 at intermediate masses and ~ 0.01 at low masses).

This population exhibits a strong dependence on the environment: the fraction of objects with radio emission increases from ~ 0.02 for underdense regions ($1 + \delta < 3$) to ~ 0.15 for overdense regions ($1 + \delta > 10$). Similarly, such trend is also found (but at a low significance level) as a function of richness of galaxy groups.

Studying the radio luminosity-stellar mass plot, we found that for luminosities lower than $\log P(\mathrm{W\,Hz^{-1}})$=23.5 there is a correlation between the two quantities, that disappears at higher powers. The correlation between stellar mass and radio luminosity is not unexpected considering the relation between the accretion on to a black hole in the ”radio mode” to the black hole mass and hot gas fraction (see equation 10 of Croton et al., 2006). As stated by Croton et al. (2006), the hot gas fraction is approximately constant for galaxies with $v_{vir} > 150$ km s^{-1} and therefore the black hole luminosity scales with the black hole mass, which correlates with the stellar mass. Interestingly, half of the objects in the low radio luminosity regime reside in low densities, while the others are in overdense regions.

The correlation disappears for radio luminosities higher than $\log L_{Radio}(\mathrm{W\,Hz^{-1}})$=23.5. Almost all of these radio luminous objects reside in overdense region. On the other hand, no difference is present in the black hole mass between high and low densities and therefore it seems that in richer environments the emission mechanism is more efficient than in low density regions.

Therefore, we can tentatively say that at low density the emission is determined by the host galaxy stellar mass and at high density by the host structure (group/cluster) in which the galaxy resides. The higher luminosities in denser environments could be caused by a greater fuel supply (due to the central cooling of the gas) and/or to the fact that also outside the galaxy there is a significant gas density to confine the radio jet. On the other hand, we already know that ellipticals at the center of galaxy groups are richer in hot gas than isolated and non-dominant ones (Helsdon et al., 2001) and this implies that a mechanism driving gas within dominant galaxies is or has been active.

This can also justify a longer time spent by the central engine in the ”switched on” status, as suggested by the increasing ratio of passive AGN to control sample as a function of density. It would be interesting to investigate whether the high density AGN have luminosities that correlate with the central cooling flow, following the relation between radio luminosity and accretion mass found by Mittal et al. (2008). Note that our findings are consistent with those of both Best (2004), Mandelbaum et al. (2009).

Finally, the difference in overdensity between radio-loud and control samples remains constant across the studied redshift range, implying that no significant evolution in this phenomenon is present.

Non-passive AGN: This is a less well-defined family. In principle, in this class one can find not only AGN but also objects such as post–starburst galaxies. In this case, radio emission disappears on a time scale of 10^8 years, which could be longer than the disappearing time of the star formation signatures in optical. However, we expect that these objects are rare because of the implied short time scales. In fact, only two of the radio detected post–starbursts of the Vergani et al. (2009) sample and one of the upper limits lie within our AGN region. This means that post-starburst galaxies contaminate our sample by 4%. The non-passive AGN population occupies a small region of the infrared color-specific star formation rate plot, which is approximately equivalent to the green valley defined in the optical bands. These galaxies are objects with spectrophotometric type earlier than Sa-Sb and applying the standard diagnostics based on the emission line ratios we found that 50% are classified as optical AGN and the remaining are star forming galaxies. The ZEST morphologies of non-passive AGN are equally divided between early types and spirals (with a $\sim$ 8% of irregulars), while the control sample has percentages of $\sim$ 60% and 40%, respectively. The radio emitting objects of this class follow the same environment distribution of the corresponding control sample galaxies and do not show the luminosity-density behaviour.

Star Forming galaxies The composite spectra of radio emitting star forming galaxies is redder than the control sample with a smaller [OII] and higher Hα equivalent width.

Considering that the radio detected star forming galaxies are objects where the star formation rate is on average higher than the undetected ones, this implies that the dust content is higher. This increase of dust extinction with increasing star formation is already known (see e.g. Pannella et al., 2009) and could justify the relation between the emission lines and the radio SFR estimators shown in the lower panel of Figure 1. The ZEST morphological classification shows that the radio detected objects tend to be of earlier type than the control sample, as found for the spectrophotometric types.

The radio emitting star forming galaxies show an apparent difference in density distribution with respect to the control sample, but we have shown that this is due to the different stellar mass distributions of the two samples. Correcting the control sample with the fraction of radio emitting objects, no differences in environment are present between radio and control sample galaxies. This is consistent with the conclusion of Kauffmann et al. (2004) that the star formation does not depend on the density for scales larger that the Megaparsec.

Acknowledgements. We acknowledge support from an INAF contract PRIN-2007/1.06.10.08 and an ASI grant ASI/COFIS/WP3110 I/026/07/0.The VLA is operated by the National Radio Astronomy Observatory, which is a facility of the National Science Foundation, operated under cooperative agreement by Associated Universities, IIlC.

References

Baldwin, J.A., Phillips, M.M., Terlevich, R. 1981, PASP, 93, 5
Bardelli, S., Venturi, T., Zucca, E., De Grandi S., Ettori, S., Molendi, S. 2002, A&A, 396, 65
Bardelli, S., Zucca, E., Bolzonella, M., et al. 2009, A&A, 495, 431
Bell, E.F. 2003, ApJ, 596, 794
Best, P.N 2004, MNRAS, 351, 70
Best, P. N., Kauffmann, G., Heckman, T. M., Ivezič, Z. 2005, MNRAS, 362, 9
Bekki, K. 1999, ApJ, 510, L15
Birzan, L., Rafferty, D.A., McNamara, B.R., Wise, M.W., Nulsen, P.E.J. 2004, ApJ, 607, 800
Bolzonella, M., Kovač K., Pozzetti, L., et al. 2009, A&A, in press arXiv0907.0013
Bondi, M., Ciliegi, P., Schinnerer, E., et al. 2008, ApJ, 681, 1129
Bongiorno, A., Mignoli, M., Zamorani, G., et al. 2009, A&A, submitted
Bruzual, G. Charlot, S. 2003, MNRAS, 344, 1000
Capak, P., Aussel, H., Ajiki, M., et al. 2007, ApJ, 172, 99
Caputi, K.I., Kovač, K., Bolozonella. M., et al. 2009, ApJ, 691, 91
Caputi, K.I., Lilly, S.J., Ausse, H., et al. 2008, ApJ, 680, 939
Chabrier, G. 2003, PASP, 115, 763
Ciliegi et al. 2009, A&A, in prep
Ciotti,L., Ostriker, J.P., Proga, D. 2009, ApJ, 699, 89
Colless, M., Dalton, G., Maddox, S., et al. 2001, MNRAS, 328, 1039
Condon, J.J. 1992, ARA&A, 30, 575
Condon, J.J., Cotton W.D., Greisen, E.W., et al. 1998, AJ, 115, 1693
Croton, D.J., Springel, V., White, S.D.M., et al. 2006, MNRAS, 365, 11
Cucciati, O., Iovino A., Kovač K., et al. 2009, A&A, submitted
Dressler, A.,1980, ApJ, 236, 351
Giacintucci, S., Venturi, T., Bardelli, S., Dallacasa, D., Zucca, E. 2004, A&A, 419, 71
Hardcastle, M.J., Evans, Croston, J.H., 2007, MNRAS, 376, 1849
Helsdon, S.F., Ponman, T.J., O'Sullivan, E.O., Forbes, D.A. 2001, MNRAS, 325, 693
Hill, G.J., Lilly, S.J. 1991, ApJ, 367, 1
Hopkins, P.F., Robertson, B., Krause, E., Hernquist, L., Cox, T.J. 2006, ApJ, 652, 107
Ilbert, O., Tresse, L., Zucca, E., et al. 2005 A&A, 439, 863
Ilbert, O., Capak, P., Salvato, M., et al. 2009, ApJ, 690, 1236
Iovino, A., Cucciati, O., Scodeggio, M., et al. 2009, A&A, in press arXiv0909.1951
Kauffman, G., Heckman, T.M., Tremonti, C., et al. 2003, MNRAS, 346 1005
Kauffmann, G., White, S., Heckman, T.M., et al. 2004, MNRAS, 353 712
Kauffmann, G., Heckman, T.M., Best, P.N. 2008, MNRAS, 384, 953
Kewley, L.J., Dopita, M.A., Sutherland, R.S., Heisler, C.A., Trevena, J. 2001, ApJ, 556, 121
Koekemoer, A. M., Aussel, H., Calzetti, D., et al. 2007, ApJS, 172, 196
Knobel, C., Lilly, S.J., Iovino, A., et al. 2009, ApJ, 697, 1842
Kovač K., Lilly, S.J., Cucciati, O., et al. 2009, ApJ, in press arXiv0903.3409
Lacy, M., Storrie-Lombardi, L.J., Sajina, A., et al. 2004, ApJS, 154, 166
Lamareille, F., Brinchmann, J., Contini, T., et al. 2009 A&A, 495, 53
Lamareille, F., Mouhcine, M., Contini, T., Lewis, I., Maddox, S., 2004, MNRAS, 350, 396
Ledlow, M.J., Owen F. 1996, ApJ, 112,9
Lilly, S.J., Le Fevre, O., Renzini, A., et al. 2007, ApJS, 172, 70
Lilly, S.J., LeBrun, V., Maier, C., et al. 2009, ApJS, 184, 218
Mandelbaum, R., Li, C., Kauffmann, G., White, S.D.M. 2009, A&A, 393, 377
Moustakas, J., Kennicutt, R.C., Tremonti, C.A. 2006, ApJ, 624, 755
Marconi, A., Hunt, L.K. 2003, ApJ, 589, L21
Miller, N.A., Ledlow, M.J., Owen F.N., Hill, J.M. 2002, AJ, 123, 3018
Mignoli, M., Zamorani, G., Scodeggio, M., et al. 2009, A&A, 493, 93
Mittal, R., Hudson, D.S., Reiprich, T.H., Clarke, T. 2008, A&A, 501, 835
Pannella, M., Carilli, C.L., Daddi, E., et al. 2009, ApJ, 698, 116
Peng, C.Y., Impey, C.D., Rix, H.W., et al. 2006, ApJ, 649,616
Pozzetti, L., Bolzonella, M., Lamareille, F., et al. 2007, A&A, 474, 433
Pozzetti, L., Bolzonella, M., Zamorani, G., et al. 2009, A&A, in press arXiv0907.5416
Salpeter, E.E. 1955, ApJ, 121,161
Sanders,D.B., Salvato, M., Haussel, H., et al. 2007, ApJS, 172, 86
Scarlata, C., Carollo, C.M., Lilly, S.J., et al. ApJS, 172, 406
Schinnerer, E., Smolčic, V., Carilli, C.L. et al. 2007, ApJS, 172, 46
Scodeggio M., Vergani D., Cucciati, O., et al. 2009, A&A, 501,21
Scoville, N,, Abraham, R.G., Aussel, H., et al. 2007,ApJS, 172, 1
Shabala, S.S., Ash, S., Alexander, P., Riley, J.M. 2008, MNRAS, 388, 625
Silverman, J.D., Kovač, K., Knobel, C., et al. 2009b, ApJ, 695, 171
Silverman, J.D., Lamareille, F., Maier, C., et al. 2009a, ApJ, 696, 396
Smolčic, V., Schinnerer, E., Scodeggio, M., et al. 2008, ApJS, 177, 14
Smolčic, V., Zamorani, G., Schinnerer, E., et al. 2009a, ApJ, 696, 24
Smolčic, V.,Schinnerer, E., Zamorani, G., et al. 2009b, ApJ, 690, 610
Smolčic, V., 2009, ApJ, 669, L43
Vollmer, B., Braine J., Balkowski, C., Cayatte V., Duschl W.J. 2001, A&A, 374, 824
Venturi, T., Dallacasa, D., Stefanachi, F. 2004, A&A, 422, 515
Vergani, D., Zamorani, G., Lilly, S.J., et al., 2009, A&Ain press arXiv0909.1968
Tasca, L., Kneib, J.P., Iovino, A., et al. 2009, A&A, 503, 379
Zucca, E., Bardelli, S., Bolzonella, M. 2009, A&A, in press arXiv0909.4674
Zucca, E., Ilbert, O., Bardelli, S., et al. 2006, A&A, 455, 879

---

[1] 1) INAF-Osservatorio Astronomico di Bologna - Via Ranzani,1, I-40127, Bologna, Italy

[2] 2) Max Planck Institut für Astronomie, Königstuhl 17, Heidelberg, D-69117, Germany

[3] 3) California Institute of Technology, MC 105-24, 1200 East California Boulevard, Pasadena, CA 91125, USA

[4] 4) INAF-Osservatorio Astronomico di Arcetri, Largo E.Fermi 5, I-50125, Firenze, Italy

[5] 5) Institute of Astronomy, Swiss Federal Institute of Technology (ETH Hönggerberg), CH-8093, Zürich, Switzerland

[6] 6) Space Telescope Science Institute, 3700 San Martin Drive, Baltimore, MD 21218, USA

[7] 7)Max-Planck-Institut für extraterrestrische Physik, D-84571 Garching, Germany

[8] 8)INAF-Istituto di Radioastronomia, Via Gobetti 101, I-40129 Bologna, Italy

[9] 9)Laboratoire d'Astrophysique de Toulouse-Tarbes, Université de Toulouse, CNRS, 14 avenue Edouard Belin, F-31400 Toulouse, France

[10] 10)Laboratoire d'Astrophysique de Marseille,Universite' d'Aix-Marseille, CNRS , 38 rue Frederic Joliot-Curie, F-13388, Marseille, France

[11] 11)European Southern Observatory, Karl-Schwarzschild-Strasse 2, Garching, D-85748, Germany

[12] 12)Dipartimento di Astronomia, Universita' di Padova, Vicolo Osservatorio 5, I-35122, Padova, Italy

[13] 13)INAF - IASF Milano, via Bassini 15, I-20133, Milan, Italy

[14] 14)INAF Osservatorio Astronomico di Brera, via Brera 28, I-20121, Milan, Italy

[15] 15) INAF - Osservatorio Astronomico di Torino, strada Osservatorio 20, 10025 Pino Torinese, Italy

[16] 16) Departement of Astronomy, University of Massachussetts, 710 North Pleasent Street, Amherst, MA 01003, USA

[17] 17)Dipartimento di Astronomia, Universit di Bologna, via Ranzani 1, I-40127 Bologna, Italy

[18] 18)LBNL & BCCP, University of California, Berkeley, CA, 94720, USA

[19] 19)Centre de Physique Theorique, Marseille, France

[20] 20)Institut d'Astrophysique de Paris, UMR 7095 CNRS, Universit Pierre et Marie Curie, 98 bis Boulevard Arago, F-75014 Paris, France

[21] 21)Argelander Institut fr Astronomie, Auf dem Hgel 71, D-53121 Bonn, Germany

[22] 22) INAF, Osservatorio di Roma, via di Frascati 33, I-00040Monteporzio Catone (RM), Italy

[23] 23)Observatories of the Carnegie Institute of Washington, Santa Barbara Street, Pasadena, CA 91101, USA

[24] 24)Institute for Astronomy, University of Hawaii, 2680 Woodlawn Drive, HI 96822, USA

[25] 25)Research Center for Space and Cosmic Evolution, Ehime University, Bunkyo-cho 2-5, Matsuyama 790-8577, Japan
[26] 26) Max-Planck-Institut für Astrophysics, D-84571 Garching, Germany
[27] 27)Instituto de Astrofisica de Andalucia, CSIC, Apdo. 3004, 18080, Granada, Spain
[28] 28)Universitats-Sternwarte, Scheinerstrasse 1, D-81679 Muenchen